Placental growth factor mediates mesenchymal cell development, cartilage turnover, and bone remodeling during fracture repair

Christa Maes,[1] Lieve Coenegrachts,[1] Ingrid Stockmans,[1] Evis Daci,[1] Aernout Luttun,[2] Anna Petryk,[3] Rajaram Gopalakrishnan,[4] Karen Moermans,[1] Nico Smets,[1] Catherine M. Verfaillie,[2] Peter Carmeliet,[5] Roger Bouillon,[1] and Geert Carmeliet[1]

[1]Laboratory of Experimental Medicine and Endocrinology, Katholieke Universiteit Leuven, Leuven, Belgium. [2]Stem Cell Institute and [3]Departments of Pediatrics and Genetics, Cell Biology, and Development, University of Minnesota, Minneapolis, Minnesota, USA. [4]Department of Diagnostic and Biological Sciences, University of Minnesota School of Dentistry, Minneapolis, Minnesota, USA. [5]Center for Transgene Technology and Gene Therapy, Flanders Interuniversity Institute for Biotechnology, Katholieke Universiteit Leuven, Leuven, Belgium.

Current therapies for delayed- or nonunion bone fractures are still largely ineffective. Previous studies indicated that the VEGF homolog placental growth factor (PlGF) has a more significant role in disease than in health. Therefore we investigated the role of PlGF in a model of semistabilized bone fracture healing. Fracture repair in mice lacking PlGF was impaired and characterized by a massive accumulation of cartilage in the callus, reminiscent of delayed- or nonunion fractures. PlGF was required for the early recruitment of inflammatory cells and the vascularization of the fracture wound. Interestingly, however, PlGF also played a role in the subsequent stages of the repair process. Indeed in vivo and in vitro findings indicated that PlGF induced the proliferation and osteogenic differentiation of mesenchymal progenitors and stimulated cartilage turnover by particular MMPs. Later in the process, PlGF was required for the remodeling of the newly formed bone by stimulating osteoclast differentiation. As PlGF expression was increased throughout the process of bone repair and all the important cell types involved expressed its receptor VEGFR-1, the present data suggest that PlGF is required for mediating and coordinating the key aspects of fracture repair. Therefore PlGF may potentially offer therapeutic advantages for fracture repair.

Introduction

Each year, some 6.2 million patients suffer a bone fracture in the United States alone. Unlike soft tissues, which repair predominantly through the production of fibrous scar tissue at the site of the injury, bone defects heal by forming new bone that is indistinguishable from uninjured bone tissue. The repair process in adults closely resembles normal development of the skeleton during embryogenesis, which occurs by intramembranous and endochondral ossification (1). Nonetheless, some aspects are different from the fetal bone-forming process, such as the contribution of inflammation, the scarcity of pluripotent stem cells/osteoprogenitor cells, and the increased prevalence of mechanical forces in adults (2–4). Generally, bone repair is a rapid and efficient process. However, in about 10% of patients fracture healing fails, and a delayed union or nonunion develops. Possible causes are impaired blood supply; excessive damage to the periosteum, which is likely an important source of osteoprogenitor cells; inadequate immobilization; and infection of the injury site. As current therapies are still mostly ineffective, a more in-depth analysis of the cellular and molecular mechanisms underlying fracture healing will offer novel opportunities for the development of new therapies for patients with a high risk of delayed- or nonunion types of fractures.

The vascular response is critical for bone healing (5). VEGF is a prime angiogenic factor but also affects nonvascular processes in the developing bone mediated by osteoblasts, osteoclasts, and chondrocytes (6–8). Accordingly, VEGF is important during fracture healing. Inhibition of VEGF activity disrupts the repair process and results in nonunions, whereas treatment with exogenous VEGF promotes bone formation and angiogenesis in several animal models (9–12). The VEGF homolog placental growth factor (PlGF) has been shown to have a more relevant role in disease than in development (13). PlGF, originally discovered in the human placenta, is widely expressed. In humans, 3 splicing isoforms exist, PlGF-1–PlGF-3, but in mice only PlGF-2 is present. This isoform binds to the receptor tyrosine kinase Flt-1/VEGFR-1 and also interacts with neuropilins and heparin. In contrast to VEGF, the role of PlGF during development is redundant, as PlGF-deficient mice are viable and fertile and do not display major abnormalities. However, loss of PlGF impairs angiogenesis in the ischemic retina, limb, and heart, in wounded skin, and in cancer, whereas administration of recombinant PlGF (rPlGF) promotes collateral vessel growth in models of myocardial and limb ischemia (13, 14). In these pathological conditions, PlGF amplifies VEGF-driven angiogenesis (13, 15) and contributes to inflammation by recruiting and activating monocytes and hematopoietic stem cells, a process mediated through VEGFR-1 (14, 16–18).

Nonstandard abbreviations used: ALP, alkaline phosphatase; FACS, fluorescence-activated cell sorting; Ihh, Indian hedgehog; MAPC, multipotent adult progenitor cell; MT1-MMP, membrane type 1–MMP; PFD, postfracture day; PFW, postfracture week; PlGF, placental growth factor; qRT-PCR, real-time quantitative RT-PCR; r, recombinant; RANKL, receptor activator of NF-κB ligand; TRAP, tartrate-resistant acid phosphatase.

Conflict of interest: The authors have declared that no conflict of interest exists.

Citation for this article: *J. Clin. Invest.* **116**:1230–1242 (2006). doi:10.1172/JCI26772.

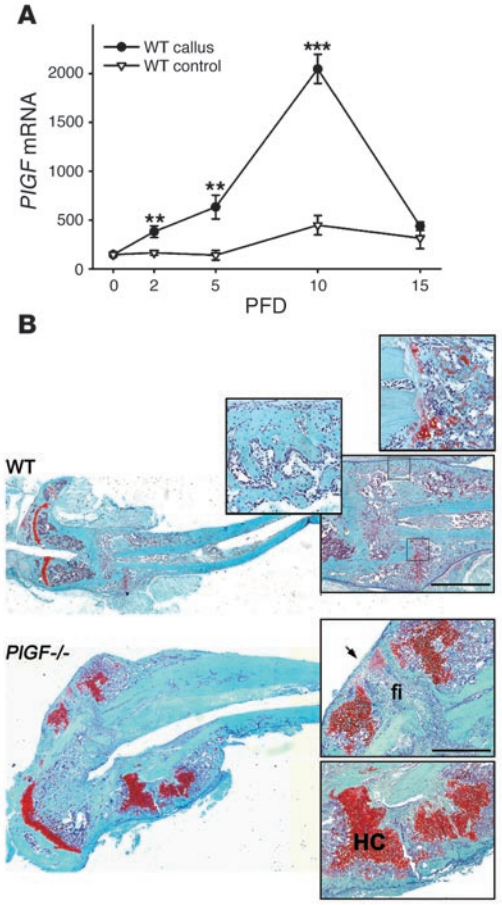

Figure 1
Impaired fracture healing in PlGF-deficient mice. (**A**) Temporal analysis by qRT-PCR of *PlGF* mRNA expression during semistabilized fracture healing in WT mice. Fracture calluses (n = 9–12) and contralateral control tissues (n = 5) were harvested at PFDs 0 (no fracture), 2, 5, 10, and 15. Values represent the number of *PlGF* mRNA copies per 1,000 copies of *hypoxanthine-guanine phosphoribosyltransferase* mRNA. $^{**}P < 0.01$; $^{***}P < 0.001$ versus control. (**B**) Safranin O staining of WT and $PlGF^{-/-}$ fractured tibia at PFD13, visualizing cartilage proteoglycans (stained red). In contrast to WT mice, $PlGF^{-/-}$ mice exhibit a large callus with massive accumulation of hypertrophic cartilage (HC), fibrous tissue (fi) at the fracture line, and lack of bony bridging (arrow). Magnified views of the WT callus show scarcely detectable cartilage and presence of bony bridging (blue lines represent callus contours). Scale bars: 1.5 mm.

Given the importance of angiogenesis and inflammation in fracture healing, we hypothesized that PlGF may also play a role in bone repair. Interestingly, primary mesenchymal stem cells with osteogenic properties and osteoblast-like MG63 cells express PlGF when stimulated by the potent osteogenic agent bone morphogenetic protein–2 (19). Furthermore, osteoblasts as well as osteoclasts express VEGFR-1 (20, 21), suggesting that PlGF may have several roles in bone regeneration beyond inflammation and angiogenesis. To address this question, we analyzed the process of bone repair in PlGF-deficient ($PlGF^{-/-}$) and WT mice.

Results

Expression of PlGF during fracture repair. To investigate the role of PlGF in bone repair we used a model of semistabilized fracture healing, which displays the established phases of fracture repair in WT mice. These include an initial inflammatory phase during the first days after fracture, a soft callus reparative phase until postfracture day 10 (PFD10), a hard callus phase between PFD10 and PFD21, and a bone-remodeling phase extending until several weeks after fracture (3).

We first monitored PlGF expression during fracture repair by real-time quantitative RT-PCR (qRT-PCR) on calluses and contralateral uninjured tissues from WT mice (Figure 1A). Immediately after fracture, at PFD2, *PlGF* mRNA expression was upregulated more than 2-fold in the callus compared with both PFD0 and PFD2 uninjured samples. PlGF expression continued to increase at PFD5 and was maximal at the transition between the soft and hard callus phases at PFD10. Subsequently, during the period of advanced bone deposition and remodeling at PFD15, *PlGF* mRNA levels in the callus declined again to baseline levels. These data indicate a rapid and strong induction of PlGF expression during fracture repair, suggesting a role for PlGF in the inflammatory and reparative phases.

Altered bone repair leading to delayed unions in PlGF-deficient mice. Fracture repair in WT and $PlGF^{-/-}$ mice was analyzed at various time points, revealing the most striking morphological difference at PFD13. The WT callus consisted mainly of woven bone, internally having a typical trabecular-like structure and externally bridging the fracture gap in all mice studied (n = 7; Figure 1B). Cartilage was scarcely detectable on safranin O–stained sections, either as small islands overlaying the cortical bone ends or in a few small regions undergoing endochondral ossification. In contrast, the $PlGF^{-/-}$ callus contained large masses of cartilage, and fibrous tissue was observed at the fracture line, discontinuing the bony bridge in 6 of 9 $PlGF^{-/-}$ mice (versus 0 of 7 WT mice; P = 0.011, Fisher's exact test). Notably, no differences in body weight or bone size or morphology were detected between the genotypes under physiological conditions (PFD0; data not shown). Thus fracture healing was impaired in mice lacking PlGF, as their calluses contained massive amounts of cartilage at a time when WT calluses were almost completely ossified, reminiscent of the clinical picture of delayed- or nonunion fractures. Further investigation was conducted to unravel the underlying mechanisms.

Impaired inflammatory response to fracture in the absence of PlGF. The inflammatory and angiogenic responses in the initial phase of fracture healing are believed to be important in triggering the repair process (4). Furthermore, a key role for PlGF in inflammation and inflammation-associated angiogenesis has been described previously (14). Given that the initial phase of fracture healing was marked by a rapid and progressive upregulation of PlGF expression in WT mice (Figure 1A), we first focused on inflammation and angiogenesis early after fracture.

As shown by immunostaining for the inflammatory cell marker CD45, the WT fracture site at PFD3 was characterized by pronounced inflammation (Figure 2A). CD45-positive cells (leukocytes) accumulated at the cortical bone ends and in the BM near the fracture line (Figure 2B) and in the surrounding soft tissues (e.g., muscle tissue). CD45 staining was strongly reduced in $PlGF^{-/-}$ mice at PFD3 (Figure 2A), which was especially evident at the site of the cortical bone fragments, where the intensity and extent of the CD45 staining areas were scored as 1.65 ± 0.16 AU for $PlGF^{-/-}$ mice versus 2.55 ± 0.28 for WT

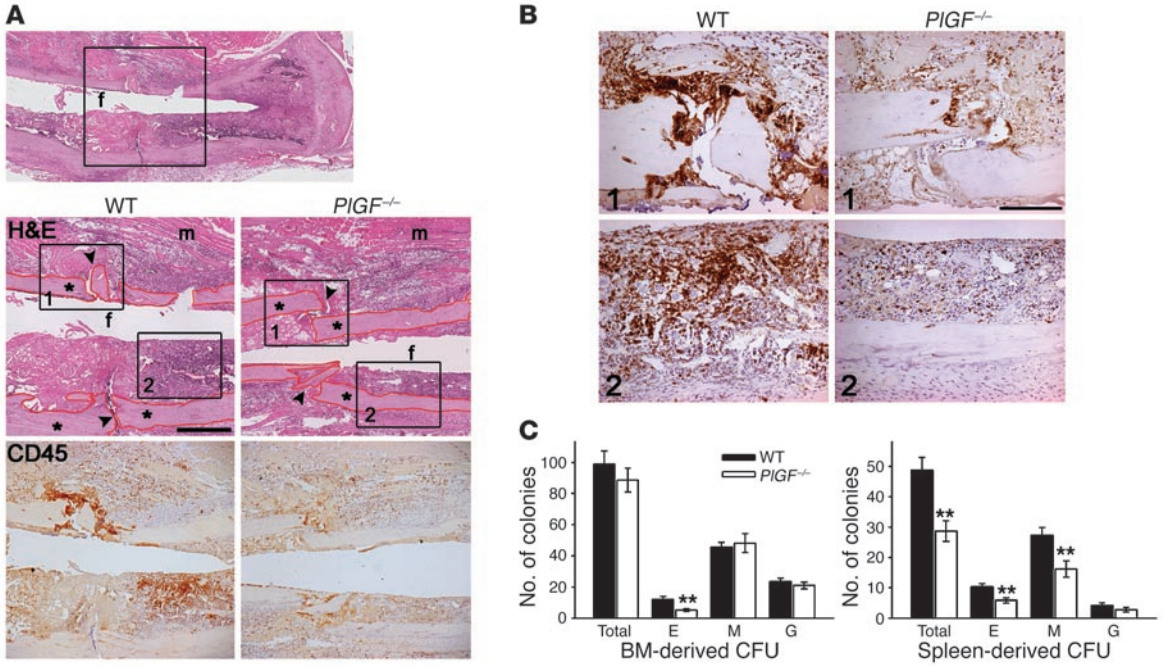

Figure 2
Reduced inflammatory reaction to trauma in the absence of PlGF. (**A**) Top panel: PFD3 WT tibia stained by H&E to visualize the fracture localization, the box corresponding to the area shown in panels below. Bottom panels: Morphology of WT and *PlGF*$^{-/-}$ calluses at PFD3 shown by H&E staining and inflammatory cell accumulation in the fracture environment shown by CD45 staining on subsequent sections. Cortical bone fragments (asterisks) are lined in red. Arrowheads indicate fracture site. m, muscle; f, fixator. Scale bar: 500 μm. (**B**) Detailed view of areas 1 and 2 boxed in **A**, showing more abundant accumulation of CD45-positive cells in WT than in *PlGF*$^{-/-}$ calluses, both on the broken cortex fragments (top panel) and in the marrow near the fracture site (bottom panel). Scale bar: 200 μm. (**C**) Hematopoietic colony-forming cell assay of BM and spleen derived from WT and *PlGF*$^{-/-}$ mice, showing the number of colonies (hematopoietic progenitor CFU) counted at day 9 of culture. E, erythroid; M, monocyte/macrophage; G, granulocyte. $^{**}P < 0.01$.

mice ($P < 0.01$, Wilcoxon test; $n = 7–10$). In addition, in none of the *PlGF*$^{-/-}$ mice ($n = 10$) was a dense focus of inflammation observed in the nearby BM, whereas this was seen in 3 of 7 WT animals ($P = 0.051$, Fisher's exact test; Figure 2B). No large differences between the genotypes were observed in the surrounding muscle tissues (Figure 2, A and B). These findings indicate that the immediate inflammatory response to fracture was impaired in the mutant calluses.

A possible explanation for this reduced inflammatory reaction is that hematopoietic progenitor differentiation potential becomes altered in the absence of PlGF. Therefore we investigated the colony-forming ability of BM and spleen hematopoietic progenitors derived from WT and *PlGF*$^{-/-}$ mice. On average, 82–85% of the formed colonies were identified as erythroid, monocyte/macrophage, or granulocyte, while the others were mixed colonies. Both BM and spleen cell cultures derived from *PlGF*$^{-/-}$ mice displayed a significantly ($P < 0.0043$ for BM and $P < 0.0030$ for spleen) reduced number of erythroid colonies compared with WT cultures at day 9 of culture ($n = 11–13$; Figure 2C). No differences were seen in the other types of colonies formed from BM cells. However, spleen cell cultures of *PlGF*$^{-/-}$ mice revealed a severely reduced total number of colonies largely due to significantly reduced CFU-monocyte/macrophage colonies (Figure 2C). Thus the impaired immediate recruitment of inflammatory cells to the fracture site of *PlGF*$^{-/-}$ mice may be explained at least in part by the reduced hematopoietic/inflammatory progenitor potential, especially of their spleen cells.

PlGF is required for the early angiogenic response to fracture. ECs accumulate at the fracture site closely following or concomitant with invasion by inflammatory cells. This angiogenic response may occur in response to cytokines and growth factors produced by the inflammatory cells, as well as to hypoxia in the fracture environment (22). In *PlGF*$^{-/-}$ mice at PFD3, the presence of CD31-immunopositive ECs in the callus was markedly reduced compared with WT mice (Figure 3A), indicating an impaired immediate vascular response. This histological observation was associated with altered mRNA expression of VEGF family members (Figure 3B). In WT mice, bone fracture induced a rapid (PFD2) and strong upregulation of VEGF expression in the callus, whereas this response was significantly reduced in *PlGF*$^{-/-}$ mice. In agreement with the delayed recruitment of inflammatory cells and ECs, which express VEGFR-1, the mRNA level of the PlGF receptor was significantly reduced in *PlGF*$^{-/-}$ fractures compared with WT at PFD2 and also remained significantly reduced during subsequent stages (PFD5 and PFD10). VEGFR-2 expression was reduced, albeit not significantly, in *PlGF*$^{-/-}$ calluses at PFD5 and PFD10 ($P = 0.06$ versus WT calluses; Figure 3B), and no significant differences between the genotypes were found in neuropilin 1 expression at any stage. These findings indicate that PlGF is indispensable for the immediate inflammatory and angiogenic response to bone trauma.

PlGF mediates proliferation and osteoblastic differentiation of mesenchymal progenitor cells. During bone repair, mesenchymal cells originating from the BM near the fracture are believed to

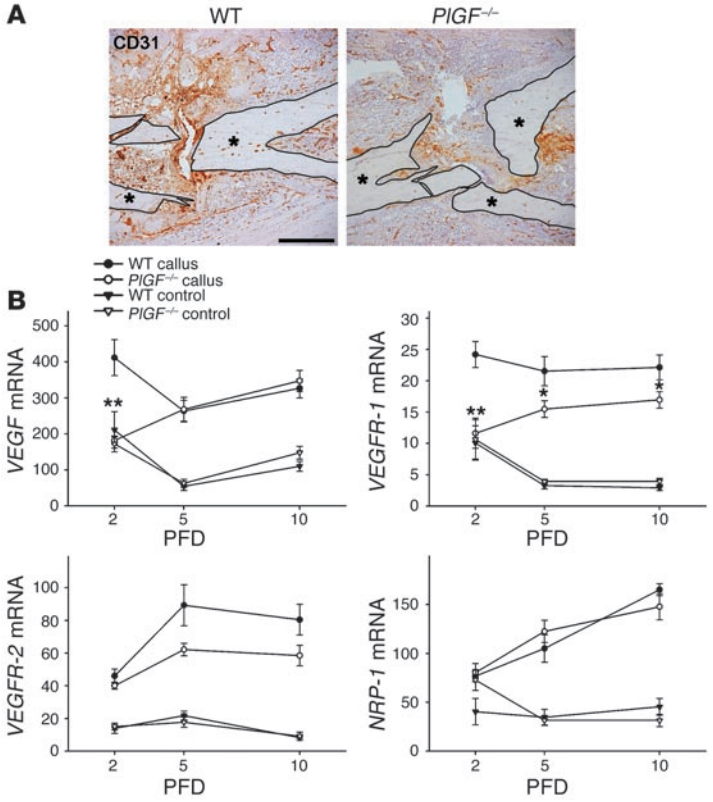

Figure 3
Reduced angiogenic reaction to fracture in the absence of PlGF. (**A**) CD31 immunostaining of WT and *PlGF*$^{-/-}$ calluses at PFD3 showing reduced accumulation of ECs in *PlGF*$^{-/-}$ mice. Cortical bone fragments (asterisks) are lined in black. Scale bar: 500 μm. (**B**) Expression levels of *VEGF*, *VEGFR-1*, *VEGFR-2*, and *neuropilin 1* (*NRP-1*) mRNA during fracture repair in WT and *PlGF*$^{-/-}$ mice, determined by qRT-PCR. The early upregulation of VEGF and VEGFR-1 expression after fracture (PFD2) was impaired in *PlGF*$^{-/-}$ mice, and *VEGFR-1* mRNA remained significantly lower in mutant calluses compared with WT calluses (PFD5–PFD10). Data are mean ± SEM. **P* < 0.05, ***P* < 0.01 versus WT callus (2-sided 2-sample Student's *t* test).

invade the wound site, proliferate, condense, and differentiate into chondrocytes or osteoblasts necessary for bone regeneration. In addition, the periosteum is considered to be another major source of mesenchymal progenitor cells. The periosteum exhibits a strong mitogenic reaction early after fracture, and its removal can delay the healing process (23, 24). As observed on H&E-stained sections (data not shown), the periosteum adjacent to the fracture site showed extensive thickening in WT mice at PFD3 but was only minimally enlarged in *PlGF*$^{-/-}$ calluses. To assess whether altered proliferation of osteoprogenitors contributed to the phenotype, we analyzed BrdU incorporation in response to fracture (Figure 4). The thickened periosteum in WT mice contained numerous proliferating cells, whereas the periosteal area was decreased by 33% in *PlGF*$^{-/-}$ mice and showed very few BrdU-stained cells (proliferation index was only 46% of WT; Figure 4, B, C, and E). BrdU-positive cells were also abundant in the BM near the fracture line in WT mice, but their number was reduced in *PlGF*$^{-/-}$ mice (Figure 4D). Characterization of the cells in the periosteal thickening of WT calluses at PFD3 revealed that they expressed *Runx2* (*Cbfa1*) mRNA, a marker of osteoblasts and/or preosteoblasts (Figure 4F). Staining with the collagen dye Sirius red showed the presence of abundant collagen fibers (Figure 4F), yet the chondrocytic collagen 2 protein was not detected at this stage by immunohistochemistry (data not shown). In contrast, osteocalcin protein was often detected within the periosteal area. Thus PlGF deficiency results in a strongly impaired early proliferative response by periosteal cells, which are putative mesenchymal osteoprogenitor cells in the fracture environment.

Besides affecting proliferation, PlGF deficiency may also impair the osteoblastic differentiation of osteochondroprogenitors, as the formation of a bony bridge was impaired in *PlGF*$^{-/-}$ mice at PFD13 (see Figure 1B). To evaluate this hypothesis, we examined multipotent adult progenitor cells (MAPCs), a subpopulation of mesenchymal stem cells derived from mouse BM (25). Under specific culture conditions MAPCs differentiated to the osteoblast lineage, as evidenced by the expression of osteoblastic markers (Figure 5A). The expression of the PlGF receptor VEGFR-1 as assessed by qRT-PCR was detectable in undifferentiated MAPCs and was significantly induced at days 7 and 14 of osteoblast differentiation, coinciding with osteocalcin expression (Figure 5, A and B) and the start of mineralization (data not shown). Treating MAPCs cultured in differentiation medium with rPlGF enhanced the expression of alkaline phosphatase (ALP) as measured at day 7 of differentiation (Figure 5C). Furthermore, mineralization of the cultures was increased at days 13 (data not shown) and 21 of differentiation (Figure 5D) by the addition of rPlGF. These findings indicate that PlGF may directly stimulate the osteoblastic differentiation of multipotent mesenchymal progenitor cells residing in the BM and/or increase the mineralization induced by these progenitor-derived osteoblasts.

Altered chondrocyte development and organization and impaired cartilage turnover in PlGF$^{-/-}$ *calluses*. Next, in order to unravel the massive accumulation of cartilage in *PlGF*$^{-/-}$ calluses (see Figure 1B), we analyzed chondrocyte development and turnover. The chondrocyte differentiation markers collagen 2, Indian hedgehog (Ihh), and collagen 10 were measured by qRT-PCR (Figure 6). In WT calluses, the mRNA expression of all 3 markers progressively increased to reach maximal levels at PFD10, after which they slowly declined. Remarkably, in *PlGF*$^{-/-}$ calluses their levels were maximal already at PFD5, resulting in a significant, 3- to 4-fold increase compared with WT callus values. Subsequently the expression of collagen 2 and Ihh dropped by PFD10 below WT levels, whereas collagen 10 expression remained high. At PFD15, the mRNA levels of the chondrocyte markers were equivalent in calluses of both genotypes (Figure 6).

Morphologically at PFD8, the callus of WT and *PlGF*$^{-/-}$ mice contained both immature and hypertrophic cartilage, as seen on safranin O–stained sections (Figure 7A). Histomorphometric analysis revealed that the total percentage of cartilage in the callus was similar in both genotypes, as were the proportions of the immature and hypertrophic cartilage regions (Figure 7B). However, the structure of the *PlGF*$^{-/-}$ and WT calluses differed. The WT callus was highly organized, consisting of mainly immature cartilage localized centrally at the fracture line and differentiating toward the peripheries, forming large hypertrophic cartilage borders orientated parallel to the fracture line and in close contact with the newly forming woven bone (Figure 7A).

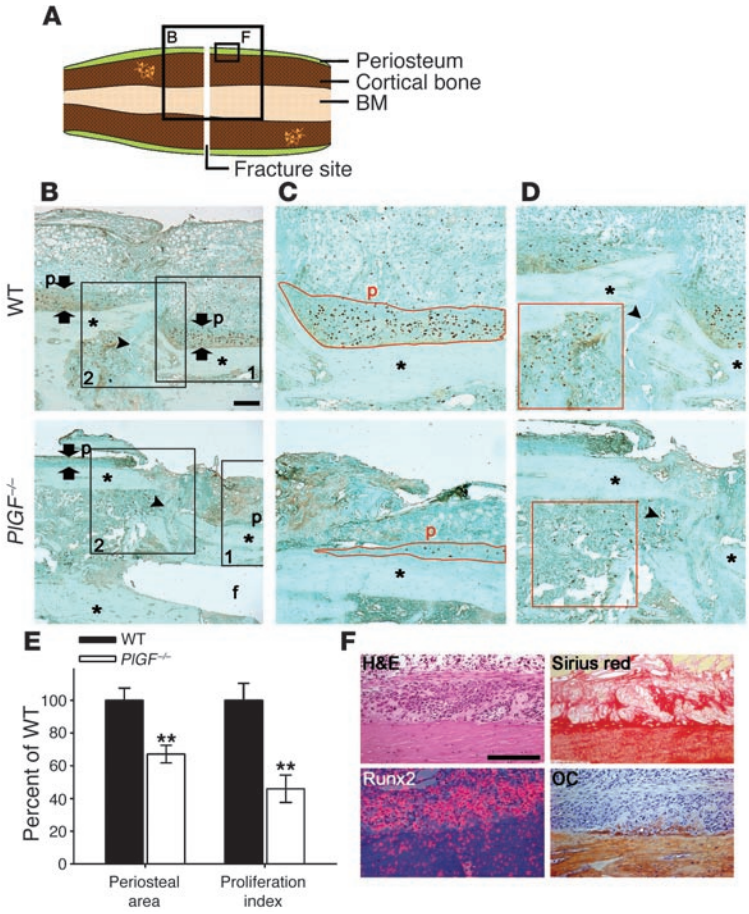

Figure 4
Impaired periosteal cell proliferation in the callus of *PlGF*$^{-/-}$ mice. (**A**) Schematic represents a fracture with boxes showing the localization of images of **B** and **F**. (**B**–**D**) Fracture calluses of WT and *PlGF*$^{-/-}$ mice at PFD3 stained for BrdU to reveal cell proliferation (brown, nuclei). Asterisks indicate cortical bone; arrowheads denote fracture site. Double arrows show thickness of the periosteal layer. p, periosteum. (**B**) Low-magnification view localizing the areas shown in **C** (box 1) and **D** (box 2). (**C**) Periosteum on the outer surfaces of the cortex fragments near the fracture site. WT mice showed strongly thickened periosteum containing abundant BrdU-positive cells, whereas *PlGF*$^{-/-}$ mice exhibited only a thin periosteal layer with scarcely detectable proliferation. (**D**) Marrow near the fracture site. In WT mice, considerable proliferation was observed internally in the callus (red box), whereas the number of BrdU-stained cells was reduced in *PlGF*$^{-/-}$ calluses. (**E**) Periosteal area and proliferation index (BrdU-positive nuclei relative to periosteal area) in WT and *PlGF*$^{-/-}$ calluses at PFD3 (as in **C**). Data are mean ± SEM. $^{**}P < 0.01$ (2-sided 2-sample Student's *t* test; $n = 6–7$). (**F**) Magnified view of the periosteal thickening of WT calluses (PFD3) examined by H&E staining, Sirius red staining, *Runx2* in situ hybridization, and osteocalcin immunostaining, showing morphology, collagen fibers, Runx2 expression, and osteocalcin protein, respectively. Scale bars: 200 μm.

In addition, the periosteum appeared to enclose the callus in a stabilizing way (data not shown). In contrast, *PlGF*$^{-/-}$ calluses were poorly organized, as evidenced by the random orientation of the fibrous and cartilaginous tissue and of the hypertrophic cartilage boundaries (Figure 7A). *PlGF*$^{-/-}$ calluses were also fragile and prone to being damaged upon tissue processing, as evidenced by multiple ruptures in the mutant sections — mostly at the interfaces between different tissue types — and torn periosteal tissues (data not shown).

Importantly, the total percentage of cartilage in the WT calluses — constituting almost 9% at PFD8 — was drastically reduced to 2% by PFD13, but this was not observed in *PlGF*$^{-/-}$ calluses (Figure 7B). This accumulating cartilage in the mutant mice consisted almost completely of viable and fully differentiated hypertrophic chondrocytes, as these regions showed *collagen 10* mRNA expression and partial matrix calcification (Figure 7C). These data suggested that chondrocyte differentiation was not impaired in the callus of *PlGF*$^{-/-}$ mice, but that the spatial organization and the turnover of the cartilage were greatly disturbed.

Vascular invasion and osteoclastic/chondroclastic degradation of cartilage. As with developmental endochondral ossification at the growth plate, hypertrophic cartilage turnover in the fracture callus depends on invasion by capillaries and osteoclasts/chondroclasts degrading the cartilage matrix. A disturbance in any of these events could explain the persistence of the hypertrophic cartilage in *PlGF*$^{-/-}$ calluses. Therefore, these processes were investigated at PFD8 (data not shown) and PFD13 (Figure 8).

Staining for CD31 revealed extensive vascularization in the callus of WT and *PlGF*$^{-/-}$ mice at PFD13. In WT mice abundant blood vessels surrounded the remnants of hypertrophic cartilage near the cortical bone fragments. Similarly, the borders of the large hypertrophic cartilage masses in the *PlGF*$^{-/-}$ callus were intensively invaded by blood vessels (Figure 8B), with no notable differences in the invading blood vessel density between the genotypes (data not shown). Analogously, tartrate-resistant acid phosphatase–positive (TRAP-positive) osteoclasts/chondroclasts abundantly accumulated at the border of the hypertrophic chondrocytes in WT as well as *PlGF*$^{-/-}$ calluses at PFD13 (Figure 8C) without any significant quantitative differences (data not shown).

A key enzyme for osteoclast/chondroclast recruitment and hypertrophic cartilage turnover during both development and repair of bone is MMP-9 (9, 26). Strong MMP-9 immunoreactivity was observed at the hypertrophic cartilage borders at PFD13, with a comparable distribution in WT and *PlGF*$^{-/-}$ mice (Figure 8D). Furthermore, no significant difference in MMP-9 expression was noted between the genotypes as measured by qRT-PCR at several time points. The expression of cathepsin K, another proteolytic enzyme of osteoclasts/chondroclasts localizing to the hypertrophic chondrocyte border (27), was also similar in *PlGF*$^{-/-}$ and WT calluses (Figure 8E). These findings indicate that the persistence of the hypertrophic cartilage in the *PlGF*$^{-/-}$ calluses is unlikely to be caused by severe alterations in vascular invasion or osteoclast/chondroclast-mediated degradation of the cartilage.

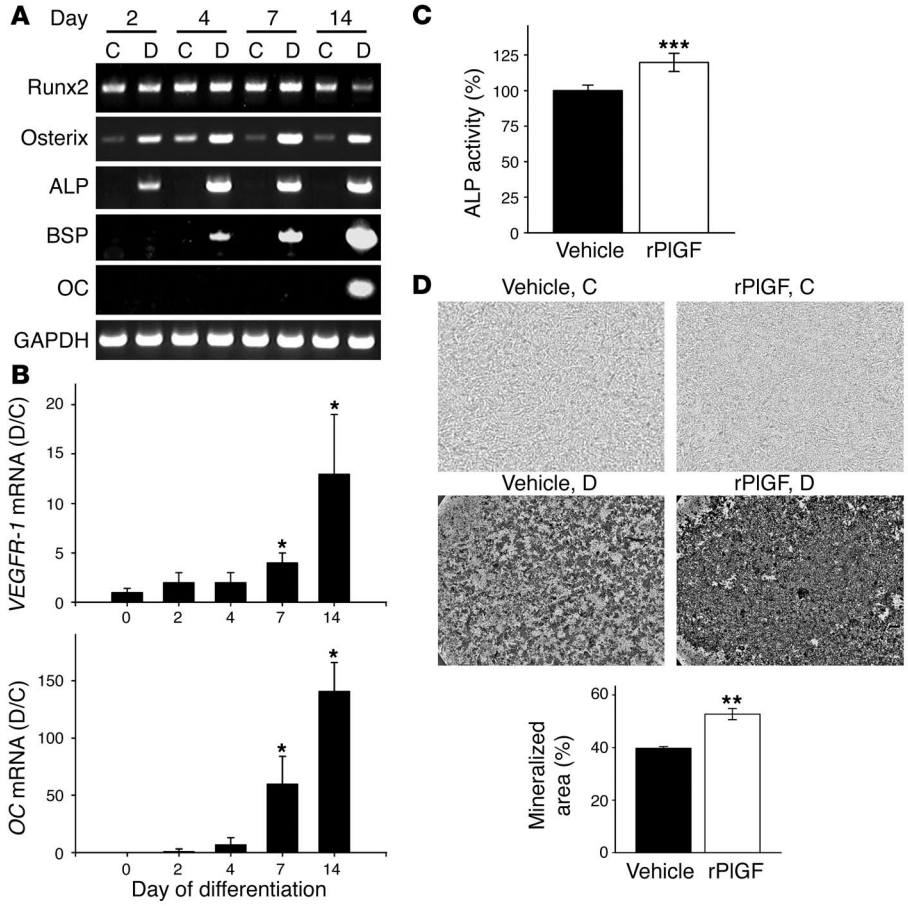

Figure 5

PlGF affects the osteoblastic differentiation of MAPCs. (**A**) Osteoblastic differentiation of mouse MAPCs cultured for 14 days in medium containing ascorbic acid (osteoblastic differentiation medium; D) compared with control medium (C). At days 2, 4, 7, and 14, the expression of the osteoblast markers Runx2, osterix, ALP, bone sialoprotein (BSP), and osteocalcin (OC) was evaluated by RT-PCR using GAPDH as a housekeeping gene. (**B**) Levels of expression of *VEGFR-1* mRNA and *osteocalcin* in MAPCs during the course of osteoblastic differentiation measured by qRT-PCR. Values are expressed as *GAPDH*-corrected levels for MAPCs cultured in differentiation medium relative to control medium for the same period. The experiment was performed 3 times. *$P < 0.05$ versus day 0. (**C**) ALP activity was significantly increased after rPlGF treatment of MAPCs cultured in differentiation medium for 7 days. Results are expressed as percentage of ALP activity in differentiating cultures incubated with vehicle. (**D**) Phase-contrast microscopy of MAPC cultures showing the effect on mineralization of adding rPlGF to the medium. At day 21, MAPCs cultured in osteoblastic differentiation medium showed extensive mineralization compared with MAPCs cultured in control medium. Mineralization was enhanced by adding rPlGF to the differentiation medium. Graph shows the quantification of the mineralized area expressed as percentage of the surface examined, revealing a significant increase by rPlGF addition. **$P < 0.01$; ***$P < 0.001$.

Reduced expression of non–osteoclast-specific collagenolytic MMPs in the fracture callus of PlGF$^{-/-}$ mice. The degradation of cartilage matrix also depends on proteolytic enzymes produced by cells other than osteoclasts/chondroclasts. Major MMPs that have been implicated in cartilage turnover during development are MMP-13, expressed by hypertrophic chondrocytes and osteoblasts (28–30), and membrane type 1–MMP (MT1-MMP), produced by osteoclasts, chondrocytes, osteoblasts, and ECs (31–33). qRT-PCR (Figure 9) revealed that at all time points examined (PFDs 2, 5, 10, and 15), the levels of *MMP-13* and *MT1-MMP* mRNA were significantly increased in WT calluses compared with the contralateral bone and reached their maximum at PFD10, indicative of a role in the repair process. Interestingly, MMP-13 expression was significantly reduced in *PlGF$^{-/-}$* calluses at this stage. Furthermore, MT1-MMP expression remained strikingly low during several stages, resulting in significantly reduced levels compared with WT calluses at PFD5 and PFD10. These data indicate impaired proteolytic activity in calluses of *PlGF$^{-/-}$* mice, which may explain the persistence of the hypertrophic cartilage masses.

Impaired bone remodeling in the absence of PlGF. Given that impaired cartilage turnover by MMP-13 or MT1-MMP deficiency results in the formation of irregular and increased bone during development (28, 30, 31), we also investigated the phase of advanced bone formation and remodeling during fracture repair.

By postfracture week 3 (PFW3), calluses of both WT and *PlGF$^{-/-}$* mice were composed almost completely of osseous tissue, without large cartilage masses, as judged on sections stained by H&E (data not shown) and safranin O (Figure 10A). However, only the *PlGF$^{-/-}$* calluses still contained safranin O–stained matrix in the woven bone, indicating the presence of remaining cartilage proteoglycans. Furthermore, the overall structure of the regenerated bone differed: in WT mice it had a typical spongy appearance enclosing abundant vascular and marrow components (Figure 10, A and B), whereas in *PlGF$^{-/-}$* calluses the bony structures were more robust, irregular, and scarcely surrounded by BM. These observations were confirmed by quantification of the collagen-rich matrix on Sirius red staining (Figure 10B): collagen constituted 53.0% ± 0.9% of the callus in WT mice versus 61.3% ± 1.9% in *PlGF$^{-/-}$* mice ($P < 0.01$; $n = 6–7$). This abnormal new bone structure was highly persistent, as 3D analysis of μCT scans at PFW8 showed that *PlGF$^{-/-}$* calluses still contained more bone than WT calluses, both in absolute terms and expressed relative to the tissue volume (Figure 10C). Accordingly, trabecular separation was significantly reduced in mutant calluses. In addition, the reduction in size of the callus and restoration to the normal shape of the tibia was impaired in *PlGF$^{-/-}$* mice: the size of the callus, determined as the size difference between the fractured and the contralateral control tibia, was significantly increased in *PlGF$^{-/-}$* mice compared with WT mice at PFW4 and PFW6 (callus area as measured on lateral X-ray views; Figure 10D) as well as PFW8 (callus tissue volume as determined by μCT analysis; Figure 10C).

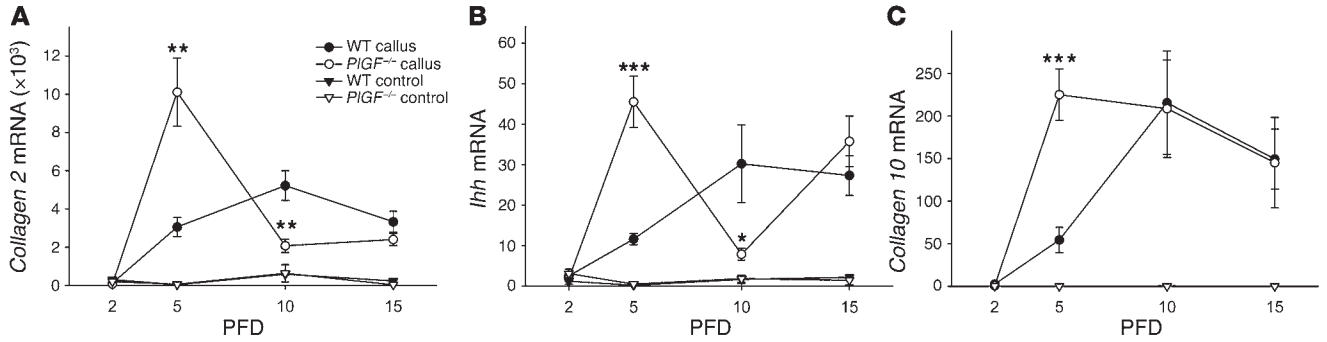

Figure 6
Expression of chondrocyte differentiation markers during fracture repair in WT and *PlGF*$^{-/-}$ mice. mRNA expression levels of (**A**) *collagen 2*, (**B**) *Ihh*, and (**C**) *collagen 10* were determined in callus and control tissues isolated from WT and *PlGF*$^{-/-}$ mice at PFDs 2, 5, 10, and 15. Shown are mean ± SEM. **P* < 0.05, ***P* < 0.01, ****P* < 0.001 versus WT callus (2-sided 2-sample Student's *t* test).

Thus *PlGF*$^{-/-}$ calluses showed altered bone structure and persistently increased size, which may be due at least in part to impaired cartilage turnover but is also indicative of a defect in the remodeling of the hard callus, a process mediated by osteoclasts. Moreover, osteoclasts express VEGFR-1 and are closely related to monocytes/macrophages, cells that are highly PlGF responsive.

No significant differences were found in the number of TRAP-positive cells in the woven bone of WT and *PlGF*$^{-/-}$ calluses at PFW3 (data not shown). However, large osteoclasts with numerous nuclei seemed more abundant in WT mice, while the TRAP-positive cells in *PlGF*$^{-/-}$ calluses appeared mostly small and flattened (Figure 10E). To investigate this issue, in vitro osteoclastogenesis was studied using cultures of BM osteoclast precursors treated with M-CSF and receptor activator of NF-κB ligand (RANKL). The formation of large, multinuclear TRAP-positive cells was greatly diminished in cultures derived from *PlGF*$^{-/-}$ mice compared with those of WT mice (Figure 10, F and G). In WT cultures more than 60% of the TRAP-positive cells contained more than 3 nuclei and were therefore considered osteoclasts, whereas in *PlGF*$^{-/-}$ cultures mono- and dinuclear TRAP-positive cells were abundantly present (about 80%; Figure 10G). Furthermore, 31% of the *PlGF*$^{-/-}$ osteoclasts contained just 3 nuclei, and only 22.5% were large osteoclasts with 6 or more nuclei (Figure 10G). In contrast, 77% of WT osteoclasts represented cells with more that 6 nuclei and 19% contained greater than 12 nuclei. Importantly, both genotypes contained a similar number of osteoclast progenitor cells in their BM, as evidenced by fluorescence-activated cell sorting

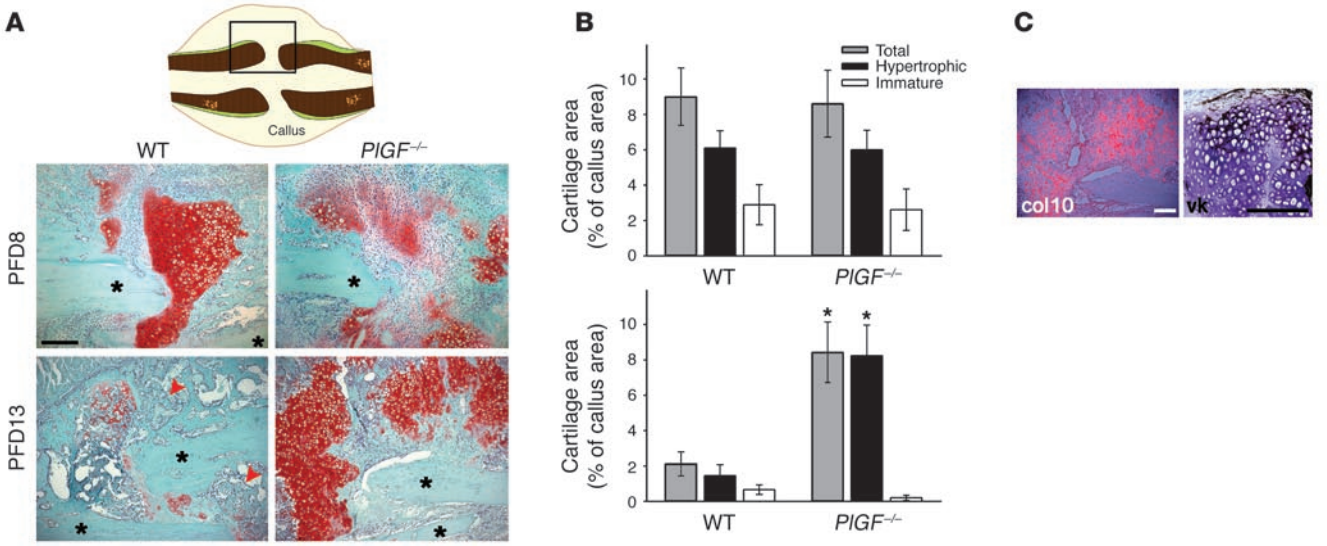

Figure 7
Altered organization and impaired turnover of callus cartilage in *PlGF*$^{-/-}$ mice. (**A**) Fracture callus demonstrating the area shown in panels below (boxed region). Safranin O staining of WT and *PlGF*$^{-/-}$ calluses at PFD8 and PFD13, showing altered cartilage organization at PFD8 and excessive cartilage accumulation at PFD13 in the mutant mice. Asterisks indicate cortical bone. (**B**) Histomorphometric analysis of callus cartilage in WT (n = 6) and *PlGF*$^{-/-}$ (n = 8) mice at PFD8 (top) and 13 (bottom). The cartilage area is expressed as percent of the total callus area, and immature (nonhypertrophic) and hypertrophic chondrocyte populations were analyzed separately. Significant differences between the genotypes were only found at PFD13, showing increased (hypertrophic) cartilage in *PlGF*$^{-/-}$ calluses. **P* < 0.05 versus WT (2-sided 2-sample Student's *t* test). (**C**) In situ hybridization for *collagen 10* (*col10*) and von Kossa staining (vk) on the cartilage accumulations in *PlGF*$^{-/-}$ calluses, showing chondrocyte viability and differentiation to the calcifying stage, respectively. Scale bars: 200 μm.

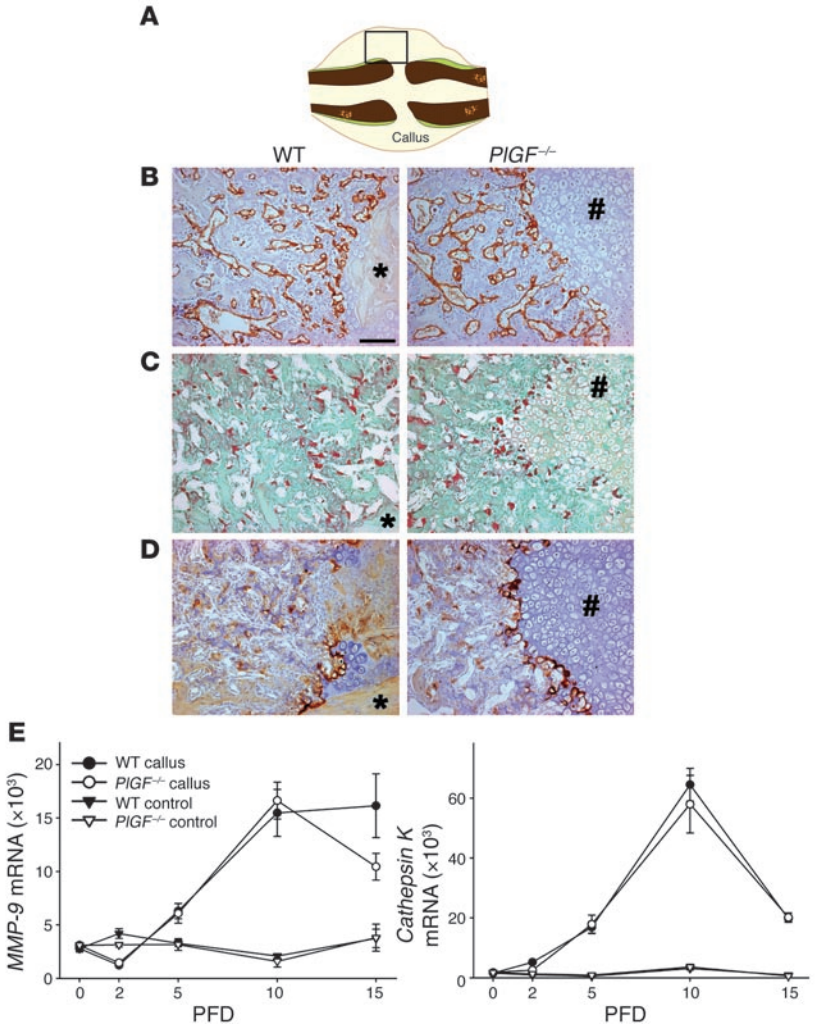

Figure 8
Endochondral ossification during fracture healing. (**A**) Fracture callus demonstrating the area shown in panels below (boxed region). (**B**–**D**) Key aspects of endochondral ossification were analyzed histologically at PFD13 in calluses of WT and *PlGF*$^{-/-}$ mice: (**B**) vascularization (CD31 staining), (**C**) presence of osteoclasts/chondroclasts (TRAP staining), and (**D**) MMP-9 protein expression and localization (immunostaining). Capillaries, osteoclasts/chondroclasts, and MMP-9 were abundant at the border of the hypertrophic cartilage (present as cartilage remnants near the cortex fragments in WT mice and as cartilage masses in *PlGF*$^{-/-}$ mice; shown as asterisks and pound symbols, respectively, at right side of images), as well as between and on the new bone trabeculae (left side). Scale bar: 100 μm. (**E**) mRNA expression levels of the osteoclastic/chondroclastic enzymes MMP-9 and cathepsin K in callus and control tissues from WT and *PlGF*$^{-/-}$ mice at PFD0–PFD15, revealing no significant differences between the genotypes.

(FACS) analysis quantifying the CD11b^{+}, Gr1^{low} osteoclast progenitor population (14.34% ± 0.96% of gated life cells in WT mice versus 17.03% ± 0.93% in *PlGF*$^{-/-}$ mice; NS). These findings suggest that the development to fully differentiated osteoclasts containing multiple nuclei is impaired in *PlGF*$^{-/-}$ mice, which could well explain the remodeling defect in their calluses.

Discussion

In this study, we discovered that the VEGF homolog PlGF was essential for normal fracture healing. In mice lacking PlGF, the callus contained massive amounts of cartilage for a prolonged period of time, reminiscent of a delayed-union type of clinical fracture, and showed defective bone remodeling in the long term. Fracture healing is complex, recapitulating aspects of developmental bone formation in combination with an inflammatory reaction, and PlGF regulated several important steps of this process (Figure 11).

Our data show that PlGF is indispensable to initiate the inflammatory response after fracture. This agrees with previous studies indicating that PlGF is crucial in inflammation-driven disorders like atherosclerosis and rheumatoid arthritis and stimulates monocyte/macrophage infiltration, differentiation, and/or activation (14, 16). Our data showing that the CFU-monocyte/macrophage population of spleen-derived hematopoietic progenitors was reduced in *PlGF*$^{-/-}$ mice further underscore the monocyte/macrophage-stimulatory effect of PlGF. A direct role of PlGF is further supported by its early increased expression in WT calluses and by the expression of its receptor VEGFR-1 on monocytes/macrophages (16). Macrophages infiltrate the fracture site early after trauma and likely initiate secondary responses. Recently, the importance of the inflammatory reaction has been underscored, as normal fracture healing was delayed in mice lacking COX-2 or the receptors for TNF-α (34, 35).

The importance of angiogenesis for fracture healing has been reconfirmed in recent studies highlighting the role of VEGF. Inhibition of VEGF activity disrupted the repair process, whereas VEGF treatment promoted angiogenesis and bone formation in several animal models and rescued the defective fracture repair in MMP-9–deficient mice (9–12). Our study also shows that PlGF deficiency impaired the initial angiogenic response in fracture repair. A possible explanation is the lack of early VEGF induction in the *PlGF*$^{-/-}$ callus, suggesting that angiogenesis at the fracture site may be mediated by VEGF but dependent on PlGF to induce VEGF either directly or indirectly via inflammatory cytokines. Another possibility, although not mutually exclusive, is that the mutant mice lack essential interactions between PlGF and VEGF, as PlGF can amplify VEGF-driven angiogenesis under pathological conditions. Finally, PlGF itself can also directly affect EC proliferation and/or differentiation as well as recruit VEGFR-1–positive (VEGFR-2–negative) ECs and hematopoietic progenitor cells from the BM, as seen in models of ischemia and myelosuppression (13, 14, 17). Analogous processes may occur at the fracture site, as vessel disruption results in local ischemia and the BM is partly ablated by the insertion of the intramedullary pin. Accordingly, the expression of VEGFR-1, but not of VEGFR-2, was reduced particularly in early *PlGF*$^{-/-}$ calluses.

Notably, vascularization was rather normal in *PlGF*$^{-/-}$ calluses at later stages, suggesting that angiogenesis during new bone formation is regulated by other factors, possibly VEGF, whose expression

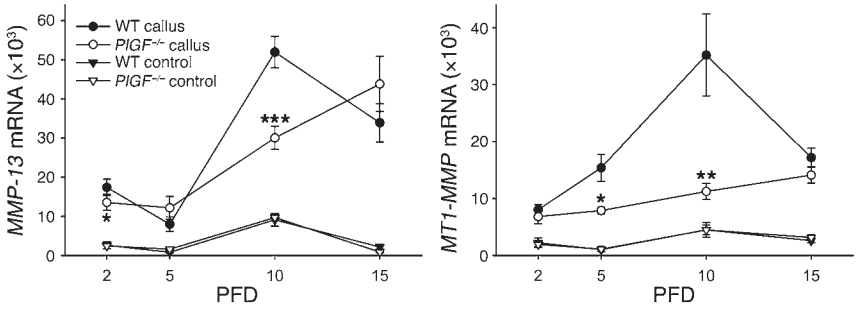

Figure 9
Reduced expression of MMP-13 and MT1-MMP in *PlGF*$^{-/-}$ calluses. The mRNA expression levels of *MMP-13* and *MT1-MMP* in callus and control tissues from WT and *PlGF*$^{-/-}$ mice at PFDs 2, 5, 10, and 15. Note significant reductions of *MMP-13* at PFD2 and PFD10 and of *MT1-MMP* at PFD5 and PFD10 in *PlGF*$^{-/-}$ versus WT calluses (*$P < 0.05$, **$P < 0.01$, ***$P < 0.001$; 2-sided 2-sample Student's *t* test).

level was restored in the mutant from PFD5 onward (see below). Moreover, the finding that PlGF was particularly involved in the immediate injury-induced angiogenic response corresponds well to its reported role in pathological settings.

During bone regeneration, mesenchymal cells proliferate and differentiate along a cartilaginous or osteoblastic lineage in response to growth factors and cytokines. The sources of these mesenchymal progenitors are still enigmatic, but the neighboring BM and periosteum are the most likely, as obliterating the BM cavity or removing the periosteum delays fracture healing (1, 2).

In WT mice at PFD3, the periosteum near the fracture line showed strong thickening, abundant cell proliferation, and expression of osteoblast markers, supporting its role as osteoprogenitor source. By sharp contrast, the periosteal layer in *PlGF*$^{-/-}$ mice was thin with only sparse proliferation. Although less pronounced, proliferation in the adjacent BM was also reduced. Despite the reduced proliferation in *PlGF*$^{-/-}$ mice, a rapid and strong induction of chondrogenesis was observed during the intermediate stages of repair, as supported by expression analysis of collagen 2, Ihh, and collagen 10, markers of increasing chondrocyte differentiation. These findings suggest that PlGF is involved in the establishment of an adequate pool of mesenchymal progenitor cells sufficient for bone regeneration and in the differentiation of these cells toward the osteoblastic lineage.

Although the contribution of the reduced inflammatory response cannot be excluded, we propose that PlGF itself affects the proliferation and/or differentiation of mesenchymal progenitors. PlGF was already significantly upregulated in WT calluses at this early stage, and VEGFR-1 was detected on mesenchymal progenitors. Furthermore, we provide in vitro evidence for a direct role for PlGF in the osteogenic differentiation of MAPCs. Recently, human mesenchymal progenitors were also shown to respond to PlGF by chemotactic migration (36). Additionally, the impaired osteogenic differentiation may limit mechanical stability, thereby favoring healing through endochondral ossification as opposed to the predominant intramembranous healing of stable fractures (3). The observation that histological sections of mutant mice at PFD3 and PFD8 were more prone to damage than WT sections underscores this hypothesis.

The reparative phases of fracture repair recapitulate the key processes of endochondral ossification, including vascular invasion, osteoclastogenesis, proteolytic enzyme activity, and osteogenesis. In *PlGF*$^{-/-}$ mice, hypertrophic cartilage excessively accumulated and persisted in the callus for a prolonged period of time, even though blood vessels and osteoclasts/chondroclasts were recruited to and invaded its surface. This latter process is dependent on VEGF and on the osteoclast/chondroclast-derived enzyme MMP-9 during both development (26, 37) and fracture repair (9). In *PlGF*$^{-/-}$ calluses, the expression and localization of MMP-9 was normal, and the expression of VEGF was restored to WT levels by PFD5. In addition, the expression of the osteoclastic/chondroclastic cysteine protease cathepsin K was not altered. Although cathepsin K is primarily considered to be crucial for bone remodeling, its main localization during fracture healing at the hypertrophic chondrocyte border (PFD10–PFD15), similar to MMP-9, implicated a role in cartilage turnover, as also suggested by the impaired remodeling of the growth plate cartilage in *cathepsin K*–null mice (27, 38). These data suggest that in *PlGF*$^{-/-}$ calluses osteoclast/chondroclast recruitment was normal and no major alterations in their characteristic enzyme expression were found that could explain the resistance of its cartilage to degradation.

Our data, however, indicated that the cartilage turnover defect in *PlGF*$^{-/-}$ mice is mainly due to reduced expression of non–osteoclast/chondroclast-specific enzymes such as MMP-13 and MT1-MMP, which have been implicated in cartilage turnover during development. The alterations in these MMPs may involve chondrocytes, osteoblasts, chondroclasts, and other noncartilage cells in the fracture callus. MT1-MMP, produced by osteoclasts as well as chondrocytes, osteoblasts, and ECs, is essential during bone development to establish the secondary ossification centers (31–33). MT1-MMP can cleave collagens type 1 and 2, which are not cleaved by MMP-9, as well as aggrecan, gelatin, fibronectin, and laminin (39). In addition, MT1-MMP is able to activate other MMPs, including MMP-2 and MMP-13 (33), thus enhancing its proteolytic target spectrum. MMP-13 has several cartilage-related collagens as substrates, including types 2, 9, and 10, and has been implicated in hypertrophic cartilage degradation during bone development (28–30). In support of an important role of these MMPs in fracture repair, their expression was strongly upregulated in calluses (compared with baseline), reaching the highest levels when active cartilage turnover occurs (our present results and ref. 40).

At later stages, the new bone formed in *PlGF*$^{-/-}$ mice appeared robust and irregular with increased resistance to callus size reduction. Defective cartilage remodeling by MMP-13 or MT1-MMP deficiency results in the formation of irregular and increased bone during development (28, 30, 31) and analogously may contribute to the abnormal structure of the bony callus in *PlGF*$^{-/-}$ mice. In support of this hypothesis, cartilage proteoglycans were visible within the woven bone of only the mutant mice at PFW3, indicating that cartilage was inadequately resorbed. However, given the endurance of the defect (at least until PFW8), a more specific bone remodeling problem is likely involved as well. The remodeling phase is mainly characterized by osteoclastic resorption aimed to reduce the size of the callus and restore the bone's original structure. Osteoclasts express VEGFR-1, and PlGF stimulates

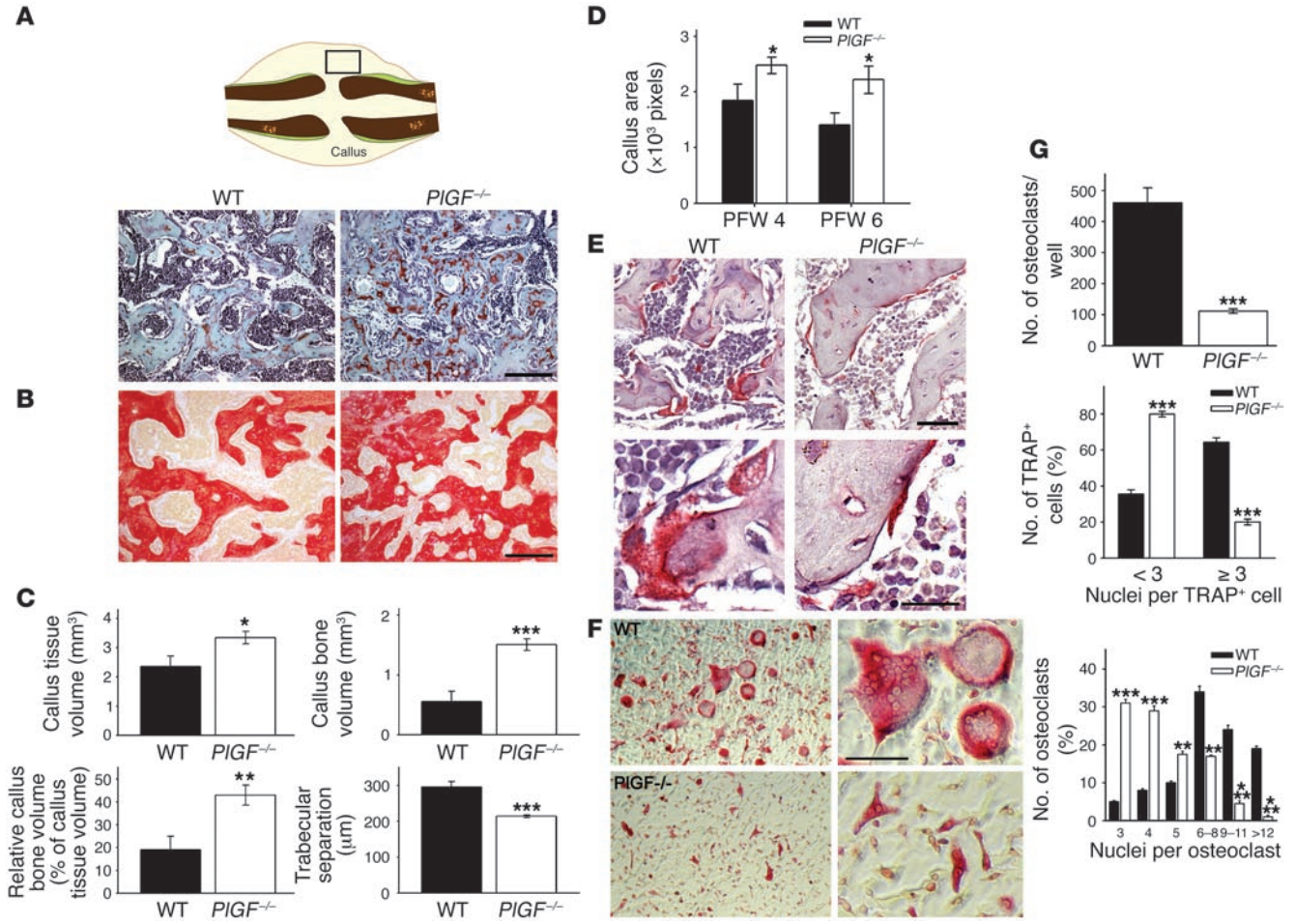

Figure 10

Impaired bone remodeling in the absence of PlGF. (**A**) Fracture callus demonstrating the area shown in panels below (boxed region). Magnified views of WT and *PlGF*$^{-/-}$ calluses at PFW3 stained by safranin O. Red-stained cartilage proteoglycans were barely detectable within the woven bone in WT but abundant in *PlGF*$^{-/-}$ calluses. Also, woven bone in *PlGF*$^{-/-}$ mice was poorly surrounded by BM. (**B**) Sirius red staining at PFW3 showed that trabecular structures in *PlGF*$^{-/-}$ calluses were more robust and irregular than those in WT calluses. (**C**) 3D analysis of μCT scans of fractured tibias at PFW8 (n = 8–10). (**D**) Quantification of callus size at PFWs 4 and 6 based on digital X-rays. (**E**) TRAP staining of calluses at PFW3 showed smaller TRAP-positive cells in *PlGF*$^{-/-}$ mice versus WT. Bottom panels show magnified views. (**F**) Representative images of in vitro osteoclast formation using cultures of BM osteoclast progenitor cells treated with M-CSF and RANKL, showing impaired formation of large, multinuclear TRAP-positive cells in *PlGF*$^{-/-}$-derived cultures compared with WT. (**G**) Quantification of in vitro osteoclast formation assays, confirming the reduced number of osteoclasts defined as TRAP-positive cells containing 3 or more nuclei (top), the increased proportion of mono- and dinuclear TRAP-positive cells (middle), and the decreased number of osteoclasts with large number of nuclei (bottom) in *PlGF*$^{-/-}$ cultures compared with WT (**P < 0.01, ***P < 0.001; 2-sided 2-sample Student's t test). Scale bars: 150 μm (**A** and **B**), 50 μm (**E**, top panels), 25 μm (**E**, bottom panels), 500 μm (**F**).

osteoclast recruitment in vivo (21). Although bone remodeling was reduced, the presence of TRAP-positive cells was not manifestly impaired in *PlGF*$^{-/-}$ calluses compared with WT mice. Yet the TRAP-positive cells in the *PlGF*$^{-/-}$ calluses appeared generally smaller and more flattened. These observations were underscored by in vitro osteoclastogenesis analyses. The number of osteoclast progenitors was not altered in *PlGF*$^{-/-}$ BM, and these cells formed abundant mono- and dinuclear TRAP-positive cells in vitro in response to M-CSF and RANKL treatment. However, the differentiation into osteoclasts containing multiple nuclei was greatly impaired compared with WT cells. This feature is plausibly hard to detect in vivo but could well explain the observed remodeling defect. Taken together, our results indicate that PlGF is essential for remodeling processes during bone repair, as lack of this factor resulted in defective cartilage turnover — mainly due to reduced expression of particular resorptive enzymes such as MMP-13 and MT1-MMP — and, at later stages, impaired bone remodeling due to altered osteoclast differentiation.

In conclusion, our data indicate that PlGF is important during 4 crucial processes of bone repair (Figure 11). First, PlGF is necessary for efficient initiation of the inflammatory and angiogenic responses to trauma. Second, PlGF affects the proliferation and differentiation of mesenchymal progenitors. Third, PlGF stimulates cartilage turnover mediated by particular MMPs. Fourth, PlGF is required for optimal remodeling of the newly formed bone. Collectively, these aspects act to establish a delayed-union fracture in *PlGF*$^{-/-}$ mice. As

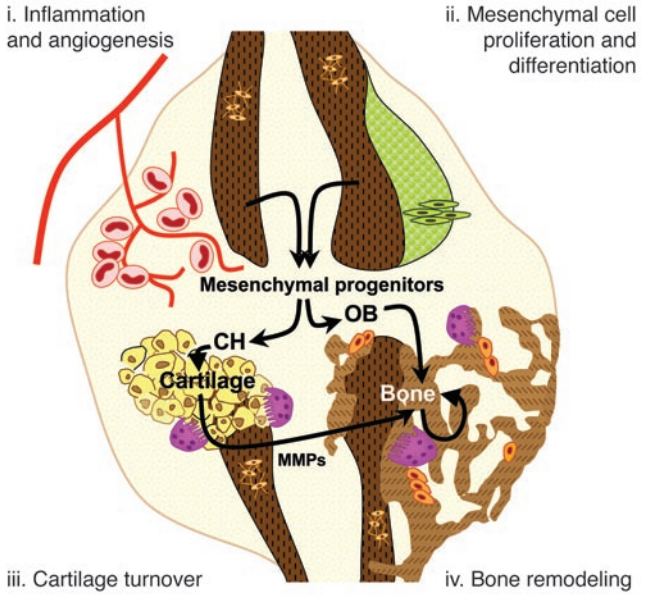

Figure 11
Schematic model of the role of PlGF in fracture healing. (i) Following fracture of bone, an inflammatory and angiogenic reaction is initiated, which is dependent on PlGF (see Figures 2 and 3). (ii) Proliferation of mesenchymal progenitor cells is induced in thickened periosteal tissue layers, a process severely affected by PlGF deficiency (see Figure 4). Mesenchymal progenitors bear the capacity to differentiate into chondrocytes (CH) or osteoblasts (OB), forming cartilage or bone, respectively. In the absence of PlGF, osteoblastic differentiation is impaired and chondrocyte differentiation may be favored (see Figures 5 and 6). (iii) Cartilage turnover and its replacement by woven bone through endochondral ossification and (iv) the subsequent remodeling of the new bone are impaired in the absence of PlGF, presumably due to reduced expression of important MMPs and impaired osteoclast functioning, respectively (see Figures 7–10).

the important cells in these phases all express VEGFR-1 (monocytes/macrophages, ECs, mesenchymal progenitors, osteoblasts, and osteoclasts) and PlGF expression is increased throughout the repair process, the present data suggest that PlGF is required for coordinating the key aspects of bone repair. This multifunctionality and diversity of PlGF becomes especially beneficial in complex processes such as fracture healing. Interestingly, PlGF is not essential for development but becomes important in pathological conditions, opening therapeutic possibilities. Therapeutic strategies to enhance fracture healing in cases of delayed or nonunions, or in cases at high risk thereof, likely require the administration of factors that complement each other. Attention has been given to the combination of angiogenic and osteogenic factors, such as VEGF and BMP-4 (41). The current study provides strong evidence that PlGF may potentially offer additional therapeutic advantages for fracture repair.

Methods

Animals. *PlGF*$^{-/-}$ and WT mice (50% Sv129, 50% Swiss; appropriate littermates were used) were bred in our animal housing facilities (Proefdierencentrum) under conventional conditions. The animals were generated by homologous recombination in embryonic stem cells as reported previously (13). Genotyping was performed by PCR of genomic DNA extracted from tail biopsies as described previously (13). The experiments were approved by the ethical committee of the Katholieke Universiteit Leuven.

Murine model of semistabilized fracture repair. A transverse bone fracture was induced in the left tibia of 11-week-old mice under pentobarbital anesthesia (100 mg/kg i.p.). Briefly, the proximal tibia was first exposed, and transversal bore injuries were created. Next, the fracture was induced using micropincers and semistabilized by an intramedullary fixating steel pin (0.4 mm diameter) inserted via the proximal articular surface. To avoid displacement of the tibia halves, the fibula was cut at mid-diaphysis. The fracture model is described in greater detail in Supplemental Methods and illustrated in Supplemental Figure 1, (supplemental material available online with this article; doi:10.1172/JCI26772DS1). Mice were sacrificed at several time points after fracture induction, expressed as PFD or PFW.

Histology and histomorphometric analysis. For histological examination, mice were sacrificed at PFD3, PFD8, PFD13, and PFW3, and the fractured tibia was carefully isolated. Processing and staining of the bones was performed as in our previous studies (6, 7) and is outlined in Supplemental Methods. Histological and histomorphometric analysis and imaging were conducted using a Zeiss Axiovert microscope and a Kontron image analyzing system (KS400 V3.00). For histological analysis of the phenotype at PFD13, an average of 20 sections sampled in a standardized manner throughout the whole callus and stained by H&E or safranin O were examined for the abundance and spatial distribution of cartilage, for the structure of woven (trabecular-like) bone in the callus and (cortical-like) bone lining the callus, and for the presence or absence of fibrous tissue at the fracture line. When at least 1 section showed fibrous tissue at the fracture line that also extended to the external side of the callus (see Figure 1B), the mouse was considered to display discontinued bony bridging of the callus. Callus inflammation was semiquantified by scoring the CD45-positive staining on a scale from 0 (no staining) to 4 (very strong staining intensity) in specific callus areas (e.g., cortex fragments, surrounding muscles). Blind scoring was performed by 2 independent investigators. The overall score per mouse was calculated as the average of 3 sections, and 7–10 mice were analyzed per genotype. Also, the presence or absence of a dense focus of inflammation was determined in the marrow close to the fracture. Periosteal cell proliferation at PFD3 was assessed by counting the number of BrdU-positive cells relative to the periosteal surface. Measurements were performed at 8 periosteal sites per mouse for 6–7 mice per genotype. Callus area and relative amount of immature and hypertrophic cartilage were quantified on safranin O–stained sections. Capillary invasion of the hypertrophic chondrocyte border was determined on CD31-stained sections as the number of vessels on the border divided by its length (μm^{-1}). Osteoclast/chondroclast invasion of the cartilage border was quantified similarly on TRAP-stained sections. The prevalence of TRAP-positive osteoclasts in the woven bone of the callus was determined as the osteoclast surface relative to the bone surface, measured in 3 areas of fixed size per section on 2–6 sections from 4–10 mice per group. At PFW3, the relative contribution of collagen (bone; stained red) and marrow components (stained yellow) was quantified in the woven bone of the callus on Sirius red–stained sections.

Isolation of tissue RNA and qRT-PCR. Mice were sacrificed at PFDs 2, 5, 10, and 15 for analysis of gene expression. The fractured as well as the contralateral (nonfractured) tibia were carefully dissected and cleared of surrounding tissues using fine gauze tissues and microdissection scissors. The callus was isolated by cutting off the proximal and distal tibia parts using micropincers. In the same way, a diaphyseal fragment of the contralateral tibia was isolated as an uninjured control sample, corresponding in length and location to the callus site. Samples were immediately snap-frozen in liquid nitrogen. Total RNA was extracted from calluses (n = 9–12 per genotype) and control samples (n = 3–5 per genotype) with TRIZOL (Invitrogen Corp.) followed by phenol/chloroform purifi-

cation, and cDNA was synthesized from equal amounts of RNA. qRT-PCR was performed on an ABI PRISM 7700 sequence detector (Applied Biosystems) as in our previous studies (6, 7) using the specific primers and probes listed in Supplemental Table 1. Gene expression was normalized for hypoxanthine-guanine phosphoribosyltransferase (HPRT) expression as an internal control and expressed as the number of mRNA copies per 1,000 copies of *HPRT* mRNA.

μCT imaging and radiography. For μCT imaging, the high-resolution Skyscan 1172 system was used. The scanner source was set at 40 kV and 250 μA, and a 0.5-mm aluminium filter was applied. The pixel size was 6.92 μm. Serial tomograms were reconstructed from raw data using a cone beam–filtered back-projection algorithm. Fractured tibia of $PlGF^{-/-}$ (n = 10) and WT (n = 8) mice at PFW8 were scanned. Additionally, for each genotype 1 representative uninjured contralateral tibia was chosen as a control based on measurements of bone size and density (grey value) performed on digital radiographic images of all mice taken at 9 mAs and 24 kV (Embrace DM1000; Agfa). Morphometric 3D analysis was performed on a bone segment encompassing 300 images spanning about 2 mm of callus proximal and distal of the site of the fracture line using CT Analyzer software (version 1.3.2.2; SkyScan). Callus tissue volume and callus bone volume were calculated by subtracting the value for control tibia, representing the uninjured tissue and bone volumes, from the values for fractured tibias. Similarly, the callus area was determined as the size difference between the fractured and control tibias for each mouse on lateral radiographs at PFW4 and PFW6.

Hematopoietic colony-forming cell assay, FACS analysis, and osteoclast formation assay. BM cells were recovered from 11-week-old WT and $PlGF^{-/-}$ mice by flushing femoral bone shafts with 5 ml RPMI-1640 (StemCell Technologies) containing 10% FCS (Invitrogen Corp.) through a single-cell strainer. Spleen-derived single-cell suspensions were prepared by gently rubbing the freshly isolated spleen over the surface of a 40-μm cell strainer and rinsing with 5 ml RPMI-1640 containing 10% FCS. Cells were purified using Ficoll (StemCell Technologies), washed twice in PBS, and resuspended in 5 ml RPMI-1640 containing 10% FCS at 100,000 BM cells/ml and 500,000 spleen cells/ml. The cells were mixed 1:12 (vol/vol) with semisolid methylcellulose medium containing 15% FCS, 10 μg/ml insulin, 200 μg/ml transferrin, and the cytokines IL-3, IL-6, erythropoietin, and SCF (Methocult M3434; StemCell Technologies) and cultured in duplicate at 1.3 ml/35 mm dish. Colonies (>30 cells each) were counted at day 6 and 9, discriminating burst-forming unit–erythroid, CFU-monocyte/macrophage, CFU-granulocyte, and mixed colonies (CFU–granulocyte-monocyte/macrophage and CFU–granulocyte-erythroid-monocyte/macrophage-megakaryocyte). To assess the number of osteoclast precursors, single-cell suspensions derived from the BM of 12-week-old WT and $PlGF^{-/-}$ mice were incubated for 30 minutes at 4°C with R-PE–conjugated anti-CD11b antibody and FITC-conjugated anti-Gr1 antibody and analyzed by FACS (FACSort; BD Biosciences), quantifying the $CD11b^{+}$ but $Gr1^{low}$ cells. For osteoclast formation in vitro, BM cells derived from WT and $PlGF^{-/-}$ mice were plated overnight in α-MEM containing 10% FCS and 10 ng/ml M-CSF (R&D Systems). Nonadherent cells were harvested, plated at 1.25×10^5 cells/cm², and cultured with 20 ng/ml M-CSF and 100 ng/ml RANKL (PreproTech), with replacement of medium at day 4. After 6 days of culture, the cells were stained for TRAP as described previously (42). The number of TRAP-positive cells containing either less than 3 or at least 3 nuclei (the latter defined as osteoclasts) as well as the number of nuclei per osteoclast were counted using light microscopy. All quantifications were performed on 4 wells per genotype, and representative results of 4 experiments are shown.

Osteoblastic differentiation of mouse MAPCs. MAPCs were isolated from mouse BM as described previously (25). Osteoblast differentiation was induced after 45 population doublings by growing the cells on fibronectin-coated dishes in the presence of 10% FBS and incubating them with differentiation media containing 0.1 μM dexamethasone, 0.2 mM ascorbic acid, and 10 mM β-glycerophosphate for up to 24 days. Cells grown in expansion media (25) were used as control. Human rPlGF-2 (100 ng/ml; RELIATech) was freshly added every other day. Media were exchanged 50% every other day. For qRT-PCR, total RNA was isolated at days 2, 4, 7, 10, and 14 of differentiation using the RNeasy minikit (QIAGEN). Primers and probes used for qRT-PCR are listed in Supplemental Table 1. The results were expressed for each time point as ratios of gene expression in differentiated and control media and normalized with *GAPDH* as a housekeeping gene. For measurements of ALP activity and mineralization, MAPCs were plated at 45,000 cells/cm² (day 0). On day 1, media were changed to differentiation or control media. For ALP assay, MAPCs differentiated for 7 days were washed in PBS, lysed in 0.2 mM Tris, 0.004% NP-40, pH 7.4, and sonicated on ice. ALP activity was measured in cell lysates using p-nitrophenylphosphate. For assaying mineralization of differentiated MAPCs, von Kossa staining was performed after 21 days. Briefly, cells were washed, fixed in 95% ethanol for 15 minutes at 37°C, and hydrated. The plates were stained with 5% $AgNO_3$ for 1 hour at 37°C, washed with water, and exposed to bright light overnight. Quantification of calcification was performed using NIH ImageJ software version 1.36 (http://rsb.info.nih.gov/ij/) by measuring the area of calcium deposition visualized by phase-contrast microscopy, and results were expressed as percent of the examined culture dish area, a fixed area in the center of the well. All quantifications were performed in triplicate, and representative results of multiple experiments are shown.

Statistics. Comparison between quantitative data of 2 groups (WT and $PlGF^{-/-}$ mice) was done by 2-sided 2-sample Student's t test using the statistical software program NCSS Stat System (version NCSS 2000), and data were expressed as mean ± SEM. Proportions were compared using a Fisher's exact test, and scoring results were compared by a Wilcoxon test using StatXact software (version 3; Cytel Inc.). P values were considered significant at $^{*}P < 0.05$, $^{**}P < 0.01$, and $^{***}P < 0.001$.

Acknowledgments

The authors thank S. Torrekens and R. Van Looveren (Katholieke Universiteit Leuven) and Y. Jiang, M. Jarcho, and L. Lien (University of Minnesota) for assistance and G. Verbeke (Biostatistical Centre, Universitaire Ziekenhuizen Gasthuisberg, Leuven, Belgium) for advising on statistics. We are grateful to J. Lammens and J. Van Lauwe (Department of Orthopedics, Universitaire Ziekenhuizen Pellenberg, Leuven, Belgium) for sharing their expertise on the fracture model. G. Marchal, A. Similon, and H. Pauwels (Department of Radiology, Mammography, Universitaire Ziekenhuizen Gasthuisberg) and P. Salmon (Skyscan, Aartselaar, Belgium) are acknowledged for sharing equipment and expertise on bone imaging by X-ray and μCT. C. Maes is a postdoctoral fellow of the Fund for Scientific Research Flanders (FWO). A. Luttun is a postdoctoral fellow of the American Heart Association. This work was supported by the FWO (G.0229.00, G.0125.00), IWT project 40312, and GOA/2001/09.

Received for publication September 2, 2005, and accepted in revised form February 21, 2006.

Address correspondence to: Geert Carmeliet, Legendo, Onderwijs en Navorsing, Campus Gasthuisberg, Herestraat 49, B-3000, Leuven, Belgium. Phone: 32-16-345974; Fax: 32-16-345934; E-mail: geert.carmeliet@med.kuleuven.be.

1. Ferguson, C., Alpern, E., Miclau, T., and Helms, J.A. 1999. Does adult fracture repair recapitulate embryonic skeletal formation? *Mech. Dev.* **87**:57–66.
2. Bruder, S.P., Fink, D.J., and Caplan, A.I. 1994. Mesenchymal stem cells in bone development, bone repair, and skeletal regeneration therapy. *J. Cell. Biochem.* **56**:283–294.
3. Le, A.X., Miclau, T., Hu, D., and Helms, J.A. 2001. Molecular aspects of healing in stabilized and nonstabilized fractures. *J. Orthop. Res.* **19**:78–84.
4. Simon, A.M., Manigrasso, M.B., and O'Connor, J.P. 2002. Cyclooxygenase 2 function is essential for bone fracture healing. *J. Bone Miner. Res.* **17**:963–976.
5. Carano, R.A., and Filvaroff, E.H. 2003. Angiogenesis and bone repair. *Drug Discov. Today.* **8**:980–989.
6. Maes, C., et al. 2002. Impaired angiogenesis and endochondral bone formation in mice lacking the vascular endothelial growth factor isoforms VEGF164 and VEGF188. *Mech. Dev.* **111**:61–73.
7. Maes, C., et al. 2004. Soluble VEGF isoforms are essential for establishing epiphyseal vascularization and regulating chondrocyte development and survival. *J. Clin. Invest.* **113**:188–199. doi:10.1172/JCI200419383.
8. Zelzer, E., et al. 2002. Skeletal defects in VEGF(120/120) mice reveal multiple roles for VEGF in skeletogenesis. *Development.* **129**:1893–1904.
9. Colnot, C., Thompson, Z., Miclau, T., Werb, Z., and Helms, J.A. 2003. Altered fracture repair in the absence of MMP9. *Development.* **130**:4123–4133.
10. Hiltunen, M.O., et al. 2003. Adenovirus-mediated VEGF-A gene transfer induces bone formation in vivo. *FASEB J.* **17**:1147–1149.
11. Ito, H., et al. 2005. Remodeling of cortical bone allografts mediated by adherent rAAV-RANKL and VEGF gene therapy. *Nat. Med.* **11**:291–297.
12. Street, J., et al. 2002. Vascular endothelial growth factor stimulates bone repair by promoting angiogenesis and bone turnover. *Proc. Natl. Acad. Sci. U. S. A.* **99**:9656–9661.
13. Carmeliet, P., et al. 2001. Synergism between vascular endothelial growth factor and placental growth factor contributes to angiogenesis and plasma extravasation in pathological conditions. *Nat. Med.* **7**:575–583.
14. Luttun, A., et al. 2002. Revascularization of ischemic tissues by PlGF treatment, and inhibition of tumor angiogenesis, arthritis and atherosclerosis by anti-Flt1. *Nat. Med.* **8**:831–840.
15. Autiero, M., et al. 2003. Role of PlGF in the intra- and intermolecular cross talk between the VEGF receptors Flt1 and Flk1. *Nat. Med.* **9**:936–943.
16. Barleon, B., et al. 1996. Migration of human monocytes in response to vascular endothelial growth factor (VEGF) is mediated via the VEGF receptor flt-1. *Blood.* **87**:3336–3343.
17. Hattori, K., et al. 2002. Placental growth factor reconstitutes hematopoiesis by recruiting VEGFR1(+) stem cells from bone-marrow microenvironment. *Nat. Med.* **8**:841–849.
18. Pipp, F., et al. 2003. VEGFR-1-selective VEGF homolog PlGF is arteriogenic: evidence for a monocyte-mediated mechanism. *Circ. Res.* **92**:378–385.
19. Marrony, S., Bassilana, F., Seuwen, K., and Keller, H. 2003. Bone morphogenetic protein 2 induces placental growth factor in mesenchymal stem cells. *Bone.* **33**:426–433.
20. Deckers, M.M.L., et al. 2000. Expression of vascular endothelial growth factors and their receptors during osteoblast differentiation. *Endocrinology.* **141**:1667–1674.
21. Niida, S., et al. 1999. Vascular endothelial growth factor can substitute for macrophage colony-stimulating factor in the support of osteoclastic bone resorption. *J. Exp. Med.* **190**:293–298.
22. Bouletreau, P.J., et al. 2002. Factors in the fracture microenvironment induce primary osteoblast angiogenic cytokine production. *Plast. Reconstr. Surg.* **110**:139–148.
23. Iwaki, A., et al. 1997. Localization and quantification of proliferating cells during rat fracture repair: detection of proliferating cell nuclear antigen by immunohistochemistry. *J. Bone Miner. Res.* **12**:96–102.
24. Ozaki, A., Tsunoda, M., Kinoshita, S., and Saura, R. 2000. Role of fracture hematoma and periosteum during fracture healing in rats: interaction of fracture hematoma and the periosteum in the initial step of the healing process. *J. Orthop. Sci.* **5**:64–70.
25. Jiang, Y., et al. 2002. Pluripotency of mesenchymal stem cells derived from adult marrow. *Nature.* **418**:41–49.
26. Vu, T.H., et al. 1998. MMP-9/gelatinase B is a key regulator of growth plate angiogenesis and apoptosis of hypertrophic chondrocytes. *Cell.* **93**:411–422.
27. Uusitalo, H., Hiltunen, A., Soderstrom, M., Aro, H.T., and Vuorio, E. 2000. Expression of cathepsins B, H, K, L, and S and matrix metalloproteinases 9 and 13 during chondrocyte hypertrophy and endochondral ossification in mouse fracture callus. *Calcif. Tissue Int.* **67**:382–390.
28. Inada, M., et al. 2004. Critical roles for collagenase-3 (Mmp13) in development of growth plate cartilage and in endochondral ossification. *Proc. Natl. Acad. Sci. U. S. A.* **101**:17192–17197.
29. Johansson, N., et al. 1997. Collagenase-3 (MMP-13) is expressed by hypertrophic chondrocytes, periosteal cells, and osteoblasts during human fetal bone development. *Dev. Dyn.* **208**:387–397.
30. Stickens, D., et al. 2004. Altered endochondral bone development in matrix metalloproteinase 13-deficient mice. *Development.* **131**:5883–5895.
31. Holmbeck, K., Bianco, P., Chrysovergis, K., Yamada, S., and Birkedal-Hansen, H. 2003. MT1-MMP-dependent, apoptotic remodeling of unmineralized cartilage: a critical process in skeletal growth. *J. Cell Biol.* **163**:661–671.
32. Holmbeck, K., et al. 1999. MT1-MMP-deficient mice develop dwarfism, osteopenia, arthritis, and connective tissue disease due to inadequate collagen turnover. *Cell.* **99**:81–92.
33. Zhou, Z., et al. 2000. Impaired endochondral ossification and angiogenesis in mice deficient in membrane-type matrix metalloproteinase I. *Proc. Natl. Acad. Sci. U. S. A.* **97**:4052–4057.
34. Gerstenfeld, L.C., et al. 2003. Impaired fracture healing in the absence of TNF-alpha signaling: the role of TNF-alpha in endochondral cartilage resorption. *J. Bone Miner. Res.* **18**:1584–1592.
35. Zhang, X., et al. 2002. Cyclooxygenase-2 regulates mesenchymal cell differentiation into the osteoblast lineage and is critically involved in bone repair. *J. Clin. Invest.* **109**:1405–1415. doi:10.1172/JCI200215681.
36. Fiedler, J., Leucht, F., Waltenberger, J., Dehio, C., and Brenner, R.E. 2005. VEGF-A and PlGF-1 stimulate chemotactic migration of human mesenchymal progenitor cells. *Biochem. Biophys. Res. Commun.* **334**:561–568.
37. Gerber, H.P., et al. 1999. VEGF couples hypertrophic cartilage remodeling, ossification and angiogenesis during endochondral bone formation. *Nat. Med.* **5**:623–628.
38. Gowen, M., et al. 1999. Cathepsin K knockout mice develop osteopetrosis due to a deficit in matrix degradation but not demineralization. *J. Bone Miner. Res.* **14**:1654–1663.
39. Sternlicht, M.D., and Werb, Z. 2001. How matrix metalloproteinases regulate cell behavior. *Annu. Rev. Cell Dev. Biol.* **17**:463–516.
40. Lehmann, W., et al. 2005. Tumor necrosis factor alpha (TNF-alpha) coordinately regulates the expression of specific matrix metalloproteinases (MMPS) and angiogenic factors during fracture healing. *Bone.* **36**:300–310.
41. Peng, H., et al. 2002. Synergistic enhancement of bone formation and healing by stem cell-expressed VEGF and bone morphogenetic protein-4. *J. Clin. Invest.* **110**:751–759. doi:10.1172/JCI200215153.
42. Daci, E., Udagawa, N., Martin, T.J., Bouillon, R., and Carmeliet, G. 1999. The role of the plasminogen system in bone resorption in vitro. *J. Bone Miner. Res.* **14**:946–952.